1991ApJ...378..586H

THE ASTROPHYSICAL JOURNAL, 378:586–598, 1991 September 10
© 1991. The American Astronomical Society. All rights reserved. Printed in U.S.A.

VARIABLE INTERSTELLAR ABSORPTION TOWARD HD 72127A. II. 1981–1988[1]

L. M. HOBBS[2]
University of Chicago, Yerkes Observatory, Williams Bay, WI 53191-0258
R. FERLET[3]
Institut d'Astrophysique de Paris, 98 bis, boulevard Arago, F-75014 Paris, France
D. E. WELTY
University of Chicago, Astronomy and Astrophysics Center, 5640 South Ellis Avenue, Chicago, IL 60637
AND
G. WALLERSTEIN
Department of Astronomy, FM-20, University of Washington, Seattle, WA 98195
Received 1991 January 25; accepted 1991 March 26

ABSTRACT

The bright visual binary HD 72127 almost certainly lies within or behind the Vela supernova remnant. From 1981 to 1988, we have obtained eight new echelle spectra of HD 72127A near the Ca II K line, along with four similar spectra near the Na I D lines. In addition to the unrivaled intensity and width of this interstellar K line formed at a distance of only $d \lesssim 500$ pc, which were previously discovered by Thackeray, the spectra show clearly the unique temporal variability of the interstellar absorption along this light path, previously reported in Paper I. The new results strengthen further the hypothesis that the interstellar absorption toward this star occurs predominantly in the disturbed gas located within the SNR, in which the interstellar grains have been largely destroyed. The variable interstellar line profiles consist of at least 10 components at the K line and of at least eight, generally corresponding components at the D lines. The total column densities summed over all of these interstellar clouds, N_{tot}(Ca II) and N_{tot}(Na I), varied irregularly by $\sim$45% in 5 years and $\sim$38% in 10 years, respectively. Larger variations were seen in the column densities of two of the individual clouds; the largest of these occurred at a low radial velocity, $v_{LSR} \approx -4$ km s^{-1}.

Subject headings: interstellar: matter — nebulae: individual (Vela SNR) — nebulae: supernova remnants — stars: individual (HD 72127)

1. INTRODUCTION

On the sky, the B2 IV star HD 72127A is located near a bright filament of the Vela supernova remnant. At a spectroscopically determined distance of $\sim$500 pc, the star apparently lies either beyond, or possibly within, the SNR. Independent evidence which strongly confirms this conclusion is provided by the interstellar absorption lines observed in the star's spectrum, which almost certainly arise predominantly in gas contained within the remnant. In particular, five properties of the interstellar K line of Ca II toward HD 72127A are exceptional:

1. The great intensity of the line, $W_\lambda \approx 600$ mÅ, which is formed over a light path of only $d \lesssim 500$ pc toward a very lightly reddened star with $E(B-V) \approx 0.08$ (Thackeray 1974);
2. the line's great width, corresponding to $\Delta v \approx 100$ km s^{-1}, again at $d \lesssim 500$ pc (Thackeray 1974);
3. the line's strikingly different appearance over a linear distance of only 2500 AU, as shown by the spectrum of HD 72127 B, a binary companion 5″ away (Thackeray 1974);
4. the abnormally large column-density ratios N(Ca II)/N(Na I) deduced for five of the line's six principal components (Hobbs 1979);
5. the temporal variability of at least two of these components (Hobbs, Wallerstein, & Hu 1982; hereafter Paper I).

Characteristics 1, 2, and 5 are unique to HD 72127, to the best of our knowledge (e.g., Hobbs 1974; Blades 1976).

These results suggest that the Ca II absorption toward the star occurs predominantly in disturbed gas within which interstellar grains have been largely disrupted, with a consequent increase in the very low fraction (<1%) of interstellar calcium usually found in the gas phase. Furthermore, some features of the temporal evolution of this disruption process apparently can be directly observed along this unusual light path. On the basis of the abnormal (i.e., more nearly solar) ratios of various interstellar gaseous abundances derived from UV interstellar lines seen toward two other stars in the region of the Vela SNR, Jenkins, Silk, & Wallerstein (1976; 1984) had found previous evidence for grain destruction, although in gas moving generally at much higher LSR velocities. A survey of various interstellar lines toward 67 stars carried out by Wallerstein, Silk, & Jenkins (1980) can be consulted for a more comprehensive view of the K-line absorption over the much larger region of the sky which delineates the Gum Nebula and which also includes the smaller Vela SNR.

In view of their exceptional nature, we have continued to monitor the interstellar lines of Ca II and Na I toward HD 72127, in order to extend the original observations obtained before 1981 June and reported in Paper I. This paper describes

[1] Based in part on observations collected at the European Southern Observatory, La Silla, Chile.
[2] Guest Observer, McDonald Observatory, University of Texas.
[3] Visiting Observer, European Southern Observatory, La Silla, Chile.

© American Astronomical Society • Provided by the NASA Astrophysics Data System

1991ApJ...378..586H

the new spectra of HD 72127A acquired from 1981 November to 1988 December.

2. OBSERVATIONS

A log of the principal observations is given in Table 1. For simplicity, the spectra will be referred to here by the numbering system given in column (1). Except for spectrum 10a, the data were obtained using the respective echelle gratings in the coudé spectrographs at either the 2.7 m reflector of the McDonald Observatory or the 1.4 m CAT reflector of the European Southern Observatory on La Silla, as indicated in column (4). The various detectors used are listed in column (5). An identical instrumental setup was purposely chosen in exposures 1–6, except that an entrance slit narrower by a factor of 2 was selected in 1986, in especially good seeing. Similarly, the instrumental arrangements were identical for exposures 7–9 and exposures 12–14, respectively, except for the substitution of the CCD detector in 1988. It is important to note that an instrumental resolution corresponding to $\Delta v \lesssim 2.7$ km s^{-1} (FWHM) was chosen for all exposures except 1–5 (col. [6]). The maximum altitude attained by HD 72127 at McDonald is slightly less than 15°. The consequently poorer resolution of spectra 1–5, which was dictated by the limited exposure times and the generally poor seeing near the horizon at McDonald, must be taken carefully into account. Except for the photoelectric PEPSIOS scan which constitutes spectrum 10a, each individual exposure recorded near 5893 Å included both the D_1 and the D_2 lines, which are listed in Table 1 as spectra 11a and 11b, respectively, for example. Finally, the observer's initials are listed in column (7) of Table 1, while the identification numbers given in the last column refer to a data archive at Yerkes Observatory. Some details concerning the instrumental arrangements, the spectra, and the reduction procedures have been discussed previously, in connection with similar spectra (Hobbs 1984; Ferlet & Dennefeld 1984; Vidal-Madjar et al. 1986).

The interstellar line profiles in our reduced spectra are shown in Figures 1–4. Four of the five characteristics of this interstellar absorption which were enumerated in § 1 are immediately evident. Additional K-line spectra of HD 72127A and of HD 72127 B were obtained in 1984 June by G. W. at Cerro Tololo Inter-American Observatory, with the same equipment which had been used for this purpose in 1981 February, which was described in Paper I. Those photographically recorded results for the brighter component of the binary, which are not presented here in detail, are consistent with the more accurate K-line profiles measured from the most nearly contemporaneous spectra, numbered 4 and 5, in Figure 1.

The interstellar line profiles seen in our spectra consist of multiple components. The method of profile fitting therefore has been used to determine the heliocentric radial velocity RV, the line width parameter b, and the column density N for each distinct absorbing cloud which is required to account for the observed profiles (Vidal-Madjar et al. 1977; Welty, Hobbs, & York 1991). A Maxwellian form was assumed for the distribution of the radial velocities within each cloud. For comparison with the observational data, the resulting theoretical profiles were convolved with a triangular instrumental function or, for spectrum 10a, a Gaussian function. The respective widths Δv (FWHM) adopted for these functions are given in Table 1. The number of clouds assumed in fitting each spectrum was restricted to the minimum possible value which permitted us to account for all of the various components unambiguously present in the data. The intensities and the radial velocities of several line components vary from one exposure to another. However, the numbers of clouds required to obtain satisfactory fits to all of the spectra at the K and the D lines, respectively, are invariant, within the limits of the observational uncertainties. This result considerably simplifies the discussion of the temporally variable absorption.

3. K-LINE PROFILES

3.1. *Equivalent Widths*

For each Ca II spectrum, the empirical S/N ratio attained at the continuum and the observed total equivalent width W_λ (in

TABLE 1

OBSERVING LOG

Number (1)	Line (2)	Date (3)	Telescope (4)	Detector (5)	Δv (km s^{-1}) (6)	Observer (7)	Identification Number (8)
1	K	1981 Apr 13[a]	McD/2.7	Digicon	5.4	LMH	391/2-737
2	K	1981 Nov 14	McD/2.7	Digicon	5.4	LMH	481/2-738
3	K	1982 Nov 7	McD/2.7	Digicon	5.4	LMH	951/2-815
4	K	1983 Nov 16	McD/2.7	Digicon	5.4	LMH	1221/2-816
5	K	1984 Nov 11	McD/2.7	Digicon	5.4	LMH	1605-817
6	K	1986 Nov 7	McD/2.7	Digicon	2.7	LMH	2219-2219
7	K	1986 Nov 20	ESO/CAT	Reticon	2.5	RF	1001-1001
8	K	1987 Nov 17	ESO/CAT	Reticon	2.5	RF	1002-1002
9	K	1988 Dec 18	ESO/CAT	CCD	2.5	RF	1003-1003
10a	D1	1977 Nov 20[b]	McD/2.7	PMT	0.9	LMH	0-259
11a	D1	1981 Nov 17	McD/2.7	Digicon	2.9	LMH	633/4-740
11b	D2	1981 Nov 17	McD/2.7	Digicon	2.9	LMH	633/4-739
12a	D1	1986 Nov 27	ESO/CAT	Reticon	2.7	RF	1004-1004
12b	D2	1986 Nov 27	ESO/CAT	Reticon	2.7	RF	1004-1004
13a	D1	1987 Nov 28	ESO/CAT	Reticon	2.7	RF	1005-1005
13b	D2	1987 Nov 28	ESO/CAT	Reticon	2.7	RF	1005-1005
14a	D1	1988 Dec 20	ESO/CAT	CCD	2.7	RF	1006-1006
14b	D2	1988 Dec 20	ESO/CAT	CCD	2.7	RF	1006-1006

[a] Paper I.
[b] Hobbs 1979.

© American Astronomical Society • Provided by the NASA Astrophysics Data System

1991ApJ...378..586H

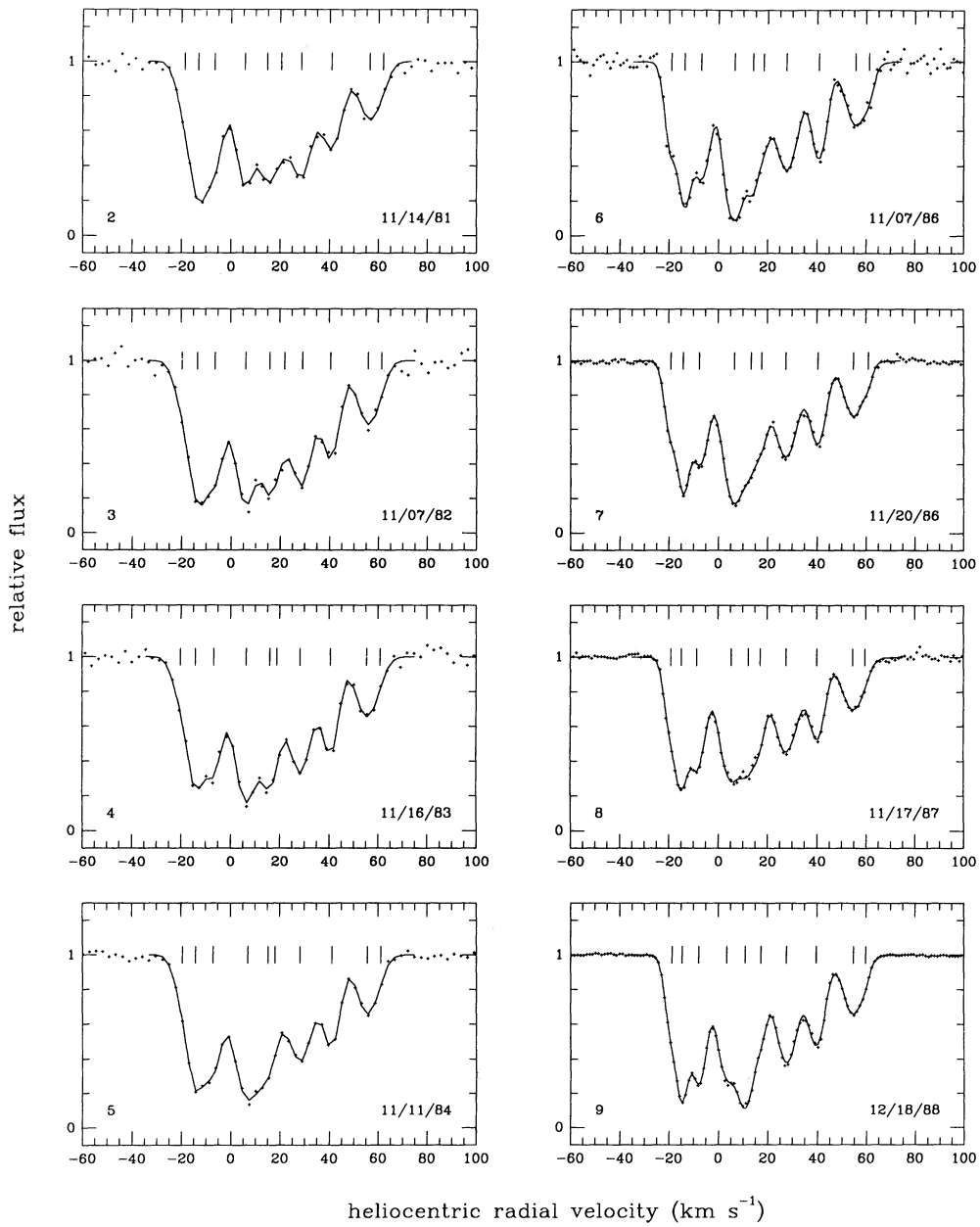

FIG. 1.—The interstellar K line of Ca II in the spectrum of HD 72127, on eight nights from 1981 through 1988. The numbering system adopted in the text identifies the respective spectra; an earlier spectrum (1981 April 13) was shown previously in Paper I. The plus signs constitute the observational data, and the solid curves are the theoretical profiles which have been fitted to the data (§ 3). The tick marks above the continua indicate the velocities of the ten line components contained in the theoretical profiles. The higher resolution of exposures 6–9 (Table 1) is very evident, especially in the case of the three components at radial velocities $\lesssim -2$ km s^{-1}; the quite different S/N ratios for the various exposures are also listed near the bottom of Table 2. The zero point for velocities measured with respect to the LSR is at a heliocentric velocity of $+16.9$ km s^{-1}.

mÅ) of the interstellar K line are given near the bottom of Table 2. For comparison, Hobbs (1974, 1978) found equivalent widths $W_\lambda \leq 310$ mÅ for all 81 stars observed at the K line in that survey, of which more than a third are at $d \gtrsim 450$ pc. The observational uncertainties in the equivalent widths for HD 72127A are also given in the table. A definite variability of this observable quantity, which amounts to $\sim 22\%$ of its average value determined from all of our spectra, is found. Over one period of slightly more than 5 years, the line's strength decreased from 628 mÅ in exposure 3, to 505 mÅ in exposure 8. A still lower value, $W_\lambda = 475$ mÅ, had been previously recorded photographically in 1977, before any of the spectra considered here were obtained (Paper I). No periodicity is distinguishable in the variation of the equivalent width toward HD 72127 in our very limited sampling of the time period in question, at roughly annual intervals. In particular, relatively large changes occur on time scales as short as 13 days, as is illustrated by a comparison of exposures 6 and 7 (§ 3.4). Therefore, excursions outside the range $505 \leq W_\lambda \leq 628$ mÅ represented in Table 2 may have occurred and gone undetected, during the time period considered here.

3.2. *Line Components*

The results of fitting the theoretical multicomponent profiles to the K line data are given in Table 2 and are illstrated in Figure 1 and in Figures 5–8. Ten distinct interstellar clouds,

© American Astronomical Society • Provided by the NASA Astrophysics Data System

1991ApJ...378..586H

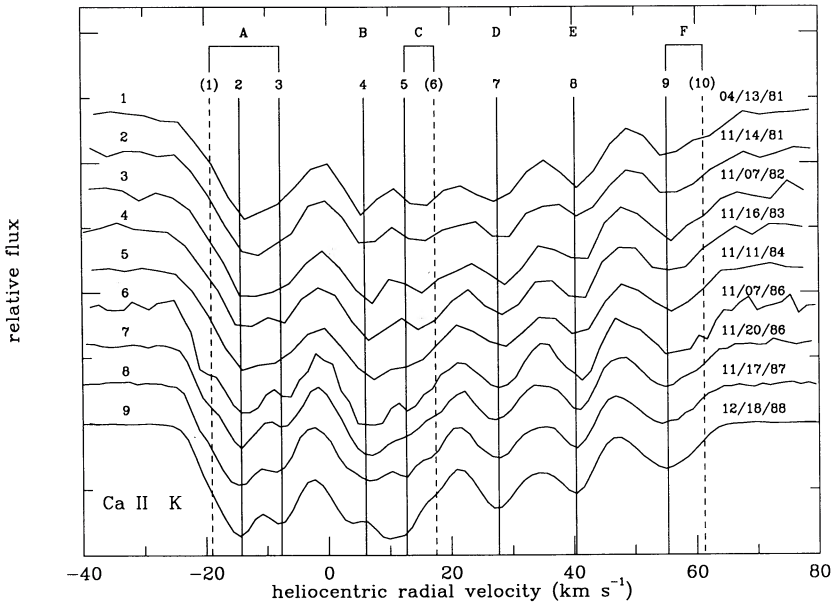

FIG. 2.—The interstellar K line toward HD 72127, on nine nights from 1981 through 1988. The solid lines connect the observed data points; these lines are *not* the theoretical line profiles of Fig. 1. The average radial velocities of the ten theoretical line components are shown by vertical lines. Dashed vertical lines are used for the three weakest, severely blended components, 1, 6, and 10. The zero level for relative fluxes in spectrum 9 is correctly shown by the bottom of the panel; each of the other eight spectra is shown to the same scale and is successively offset upward by 30% of this continuum flux.

TABLE 2

Ca II COMPONENT STRUCTURES

	EXPOSURE								
PARAMETER (1)	1981 Apr 13 (2)	1981 Nov 14 (3)	1982 Nov 7 (4)	1983 Nov 16 (5)	1984 Nov 11 (6)	1986 Nov 7 (7)	1986 Nov 20 (8)	1987 Nov 17 (9)	1988 Dec 18 (10)
N1	(4.0)	4.0 ± 1.6	3.2 ± 1.4	2.9 ± 1.0	3.1 ± 0.8	6.4 ± 0.8	4.8 ± 0.3	4.5 ± 0.7	5.4 ± 0.5
b1	(3.0)	(3.0)	(3.0)	(3.0)	(3.0)	(3.0)	(3.0)	(3.0)	(3.0)
v1	−19.3 ± 0.3	−18.5 ± 1.1	−19.6 ± 1.4	−20.1 ± 1.1	−19.5 ± 0.7	−19.0 ± 0.3	−19.1 ± 0.2	−19.2 ± 0.3	−18.8 ± 0.2
N2	23.0 ± 3.5	17.6 ± 3.6	22.1 ± 5.9	15.9 ± 2.4	16.3 ± 1.7	12.4 ± 2.4	9.6 ± 0.9	9.1 ± 1.5	12.1 ± 0.9
b2	(2.3)	(2.4)	(2.4)	(2.4)	(2.4)	2.5 ± 0.5	2.5 ± 0.2	2.5 ± 0.4	2.4 ± 0.2
v2	−13.2 ± 0.2	−13.0 ± 0.8	−13.5 ± 0.7	−14.2 ± 0.5	−14.1 ± 0.4	−13.6 ± 0.3	−14.2 ± 0.1	−14.8 ± 0.2	−14.6 ± 0.1
N3	11.8 ± 0.9	12.2 ± 1.9	15.8 ± 2.5	14.3 ± 1.4	14.0 ± 0.9	13.4 ± 2.4	11.4 ± 0.8	12.1 ± 1.2	14.1 ± 0.8
b3	(3.5)	(3.5)	(3.5)	(3.5)	(3.5)	4.5 ± 0.8	4.6 ± 0.4	4.4 ± 0.4	3.8 ± 0.3
v3	−6.1 ± 0.4	−6.5 ± 0.7	−6.4 ± 0.7	−6.7 ± 0.4	−7.1 ± 0.3	−6.9 ± 0.6	−7.5 ± 0.2	−8.6 ± 0.4	−8.0 ± 0.1
N4	19.9 ± 1.6	16.8 ± 1.9	26.5 ± 2.5	27.1 ± 1.9	30.4 ± 2.7	30.0 ± 1.9	23.7 ± 1.2	17.9 ± 1.0	15.7 ± 2.0
b4	3.1 ± 0.5	3.9 ± 1.0	4.2 ± 0.8	4.6 ± 0.6	6.2 ± 0.6	4.7 ± 0.4	5.2 ± 0.3	(5.7)	4.8 ± 0.5
v4	5.5 ± 0.2	5.8 ± 0.6	6.1 ± 0.4	6.5 ± 0.4	7.1 ± 0.5	6.7 ± 0.3	6.6 ± 0.2	5.5 ± 0.3	3.5 ± 0.4
N5	16.0 ± 2.0	12.0 ± 3.5	17.1 ± 3.8	14.7 ± 2.1	7.3 ± 2.3	8.2 ± 1.3	5.2 ± 0.8	6.7 ± 2.5	19.9 ± 2.1
b5	(3.0)	(3.0)	(3.0)	(3.0)	(3.0)	(2.5)	(3.0)	3.2 ± 1.1	3.7 ± 0.3
v5	15.0 ± 0.6	14.8 ± 1.6	15.9 ± 0.7	16.1 ± 0.5	15.2 ± 0.6	14.1 ± 0.5	13.4 ± 0.5	12.3 ± 0.6	11.0 ± 0.2
N6	(3.0)	6.0 ± 2.3	(5.0)	(2.0)	(3.0)	4.6 ± 0.9	4.6 ± 0.5	4.6 ± 1.6	4.8 ± 0.5
b6	(3.0)	(3.0)	(3.0)	(3.0)	(3.0)	(3.0)	(3.0)	(3.0)	(3.0)
v6	21.6 ± 2.7	20.5 ± 3.5	22.0 ± 2.7	(19.0)	(18.0)	18.4 ± 0.8	17.7 ± 0.3	17.2 ± 0.6	17.4 ± 0.2
N7	18.1 ± 1.6	15.5 ± 4.7	17.0 ± 2.8	17.1 ± 1.0	16.1 ± 0.7	14.5 ± 0.9	12.4 ± 0.3	12.3 ± 0.4	13.7 ± 0.3
b7	5.5 ± 0.6	4.5 ± 2.0	(4.0)	5.1 ± 0.7	6.5 ± 0.5	5.8 ± 0.5	5.9 ± 0.2	6.2 ± 0.3	5.5 ± 0.1
v7	27.8 ± 0.4	28.7 ± 1.0	29.2 ± 0.8	28.4 ± 0.3	28.2 ± 0.2	27.7 ± 0.3	27.5 ± 0.1	27.6 ± 0.1	27.7 ± 0.1
N8	10.7 ± 0.6	9.9 ± 1.5	10.7 ± 0.9	9.7 ± 0.7	8.8 ± 0.5	8.5 ± 0.4	7.2 ± 0.2	6.6 ± 0.3	8.3 ± 0.2
b8	3.3 ± 0.5	4.6 ± 1.1	3.6 ± 0.7	3.0 ± 0.6	3.2 ± 0.4	3.9 ± 0.3	4.2 ± 0.1	4.0 ± 0.2	4.3 ± 0.1
v8	41.0 ± 0.2	41.0 ± 0.7	40.6 ± 0.4	40.7 ± 0.3	41.1 ± 0.2	40.8 ± 0.2	40.4 ± 0.1	40.1 ± 0.1	39.8 ± 0.1
N9	6.6 ± 0.4	6.2 ± 0.5	6.9 ± 0.6	6.3 ± 0.5	5.9 ± 0.3	6.5 ± 0.6	5.0 ± 0.2	5.2 ± 0.3	5.7 ± 0.2
b9	6.1 ± 0.6	5.2 ± 0.7	5.1 ± 0.8	5.1 ± 0.6	4.8 ± 0.4	5.5 ± 0.6	5.0 ± 0.3	5.7 ± 0.3	5.3 ± 0.2
v9	56.2 ± 0.3	56.5 ± 0.4	55.9 ± 0.4	55.4 ± 0.4	55.6 ± 0.2	55.8 ± 0.5	54.9 ± 0.2	54.7 ± 0.3	54.8 ± 0.2
N10	(0.3)	(0.3)	(0.3)	(0.3)	(0.3)	0.6 ± 0.5	0.5 ± 0.2	0.1 ± 0.2	0.3 ± 0.2
b10	(2.0)	(2.0)	(2.0)	(2.0)	(2.0)	(2.0)	(2.0)	(2.0)	(2.0)
v10	(62.1)	(62.0)	(61.4)	(60.9)	(61.1)	61.3 ± 0.8	60.9 ± 0.4	59.7 ± 2.1	59.8 ± 0.5
S/N	35	35	30	35	60	30	100	90	165
W_λ	593 ± 14	565 ± 13	628 ± 15	592 ± 13	582 ± 7	589 ± 11	519 ± 3	505 ± 3	570 ± 2
N_{tot}	113.4	100.5	124.6	110.3	105.2	105.1	84.4	79.1	100.0
rms	0.019	0.023	0.033	0.024	0.013	0.028	0.012	0.014	0.010

© American Astronomical Society • Provided by the NASA Astrophysics Data System

1991ApJ...378..586H

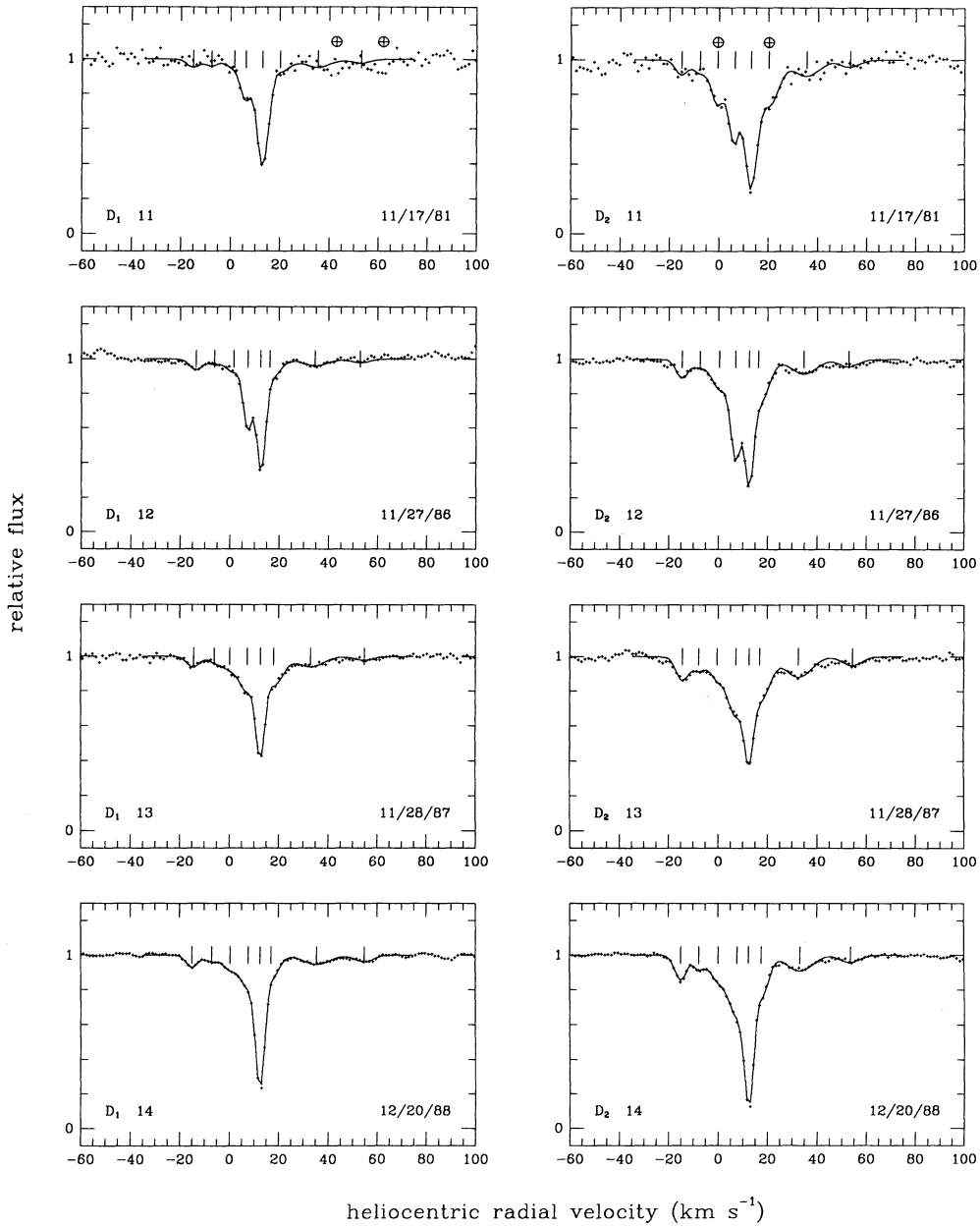

FIG. 3.—The interstellar D lines of Na I in the spectrum of HD 72127, on four nights from 1981 through 1988. The D_1 and D_2 lines are shown in the left and the right columns, respectively. The numbering system adopted in the text identifies the respective spectra; an earlier profile of the D_1 line (1977 November 20) was published previously (Hobbs 1979). The quite different S/N ratios for the various exposures are listed near the bottom of Table 3. The plus signs constitute the observational data, and the solid curves are the theoretical profiles which have been fitted to the data. Except for spectrum 11, in which the zero-point for geocentric velocities is at a helocentric velocity of 14.8 km s^{-1} and several telluric lines are indicated, any telluric lines originally present in these spectra have been removed. The tick marks above the continua indicate the velocities of the eight interstellar line components contained in the theoretical profiles. The zero point for velocities measured with respect to the LSR is at a heliocentric velocity of +16.9 km s^{-1}.

the velocities of which are shown by the tick marks above the continua in Figure 1 and by the vertical lines in Figure 2, can account for the observed Ca II absorption. Because they can be determined from our spectra less accurately than the other values, entries in Table 2 which are enclosed in parentheses were not obtained by allowing the corresponding parameter to vary completely freely, during the iterative fitting process. Such a large set of free parameters usually led to a divergence of the iterative solution, in these cases. Instead, these few parameters were fixed in advance at the values shown in the parentheses. Examples of parameters which caused this difficulty are the *b* values of the more strongly blended components in exposures 1–5, which were recorded at the lower instrumental resolution. Further examples are the various properties of the three weakest line components, numbered 1, 6, and 10, all of which are severely blended with one or more appreciably stronger components. The rms values given in the last row of Table 2 refer to the differences in the relative fluxes determined from the observed data and the theoretical profiles, calculated on a point-by-point basis across the full line profile.

The error estimates tabulated with the component parameters in Table 2 are formal uncertainties derived from the

© American Astronomical Society • Provided by the NASA Astrophysics Data System

1991ApJ...378..586H

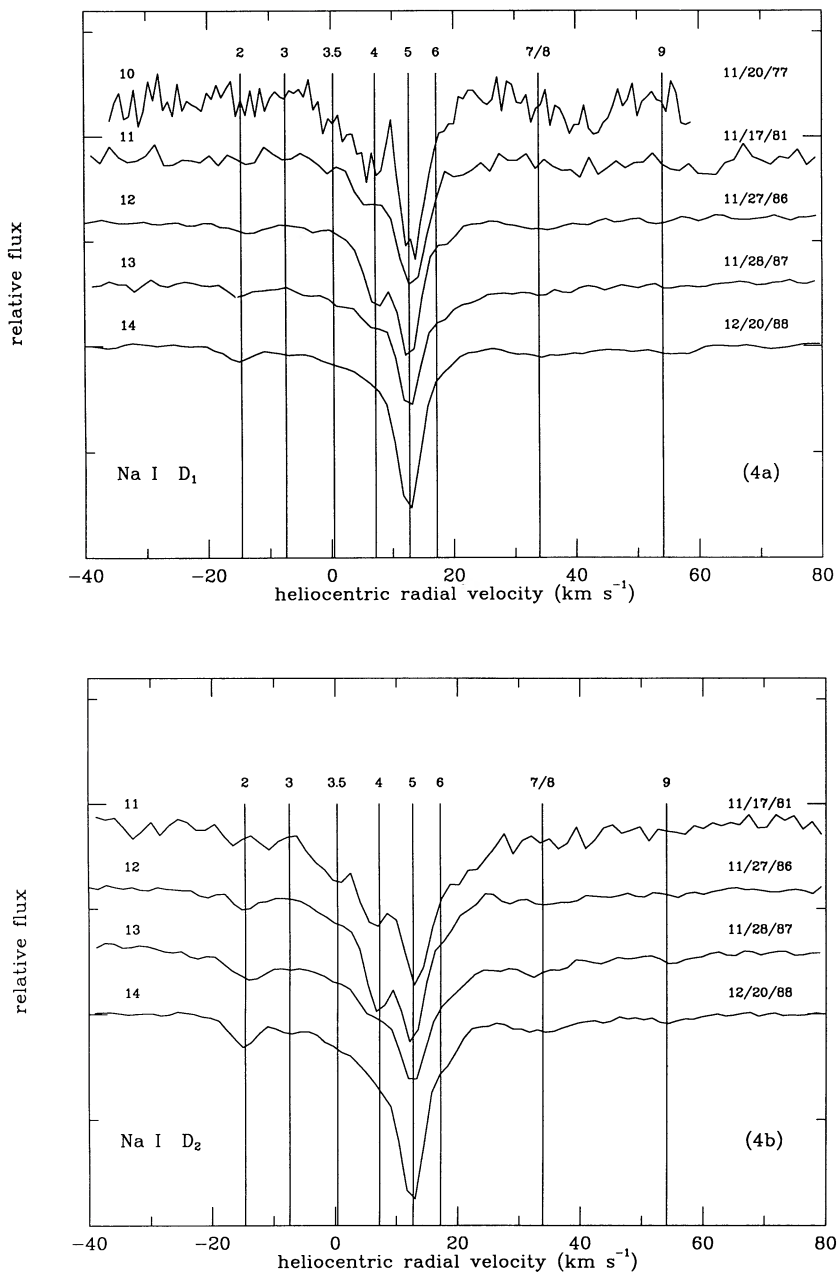

FIG. 4.—(*a*) The interstellar D_1 line toward HD 72127, on five nights from 1981 through 1988. The solid lines connect the observed data points; these lines are *not* the theoretical profiles of Fig. 3. The average radial velocities of the eight theoretical line components are shown by vertical lines. The relative fluxes are shown as in Fig. 2. (*b*) Similarly, for the D_2 line.

matrix of coefficients which is inverted to obtain parameter increments, when the fit has converged. These formal uncertainties may be considered as $\sim 1\ \sigma$ errors, since varying the best-fit parameters by 2–3 times these uncertainties yields noticeably poorer fits. These uncertainties are the random errors associated with the fitting process alone; they cannot include any possible systematic effects caused by unknown, additional errors in the zero points of intensity or in the shape or width of the assumed instrumental function, for example. The error bars shown in the various figures have been obtained by propagating these formal uncertainties in the usual way.

In view of the estimated errors in the derived velocities, it is possible that the velocity differences among components 2, 3, 7, 8, and 9 have remained constant. Holding the relative velocities of these five components fixed yielded fits that were only slightly poorer than the results actually reported here, for which the relative velocities were not constrained. The derived values of N and b were not significantly different for the two cases. Since the relative column densities of some of these five components may vary, and because there may be additional, unresolved substructure in the various line components, it would not be surprising for the relative velocities to vary as well. The results for the unconstrained fits have therefore been presented here.

© American Astronomical Society • Provided by the NASA Astrophysics Data System

1991ApJ...378..586H

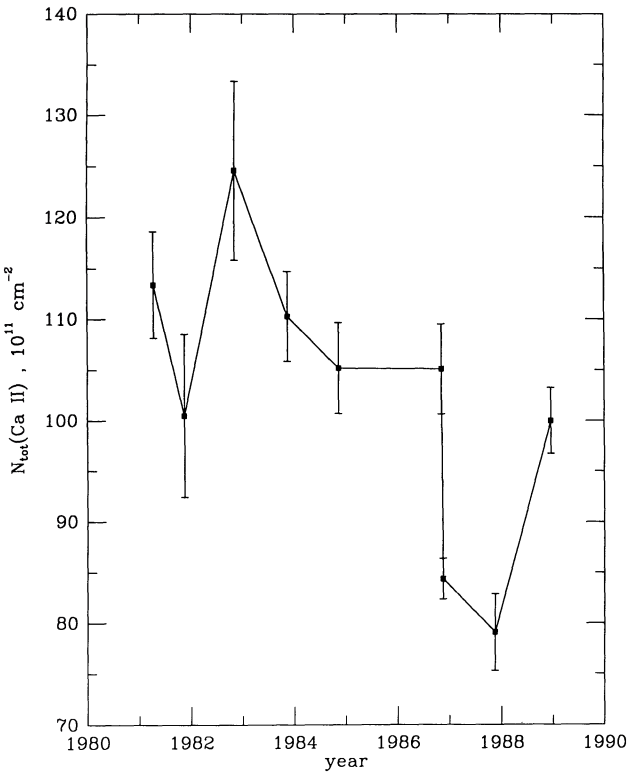

FIG. 5.—The variation with time of N_{tot}(Ca II), the total column density of interstellar Ca II along the light path to HD 72127A.

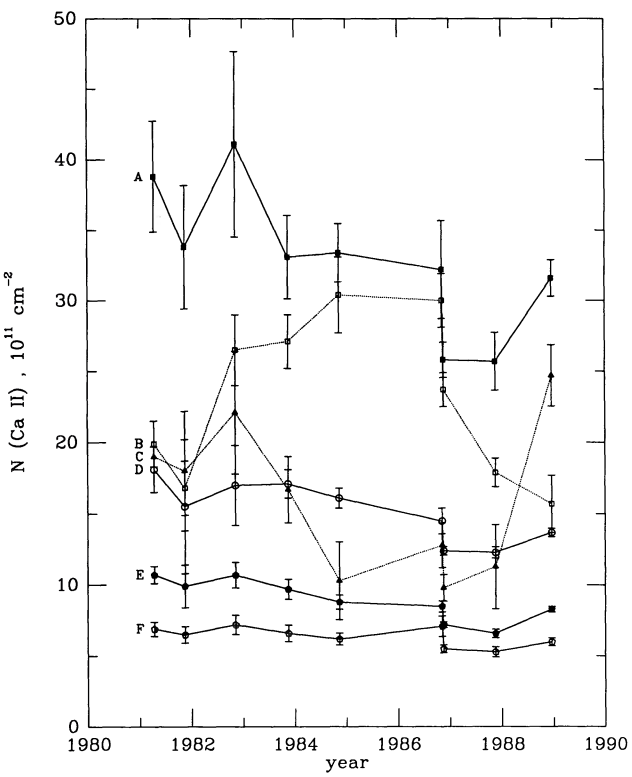

FIG. 6.—The temporal variation of the column densities N(Ca II) in the six principal kinematic groups of interstellar clouds seen at the K line. Blends A, B, C, D, E, and F are defined as the sums of components (1, 2, 3), 4, (5, 6), 7, 8, and (9, 10), respectively.

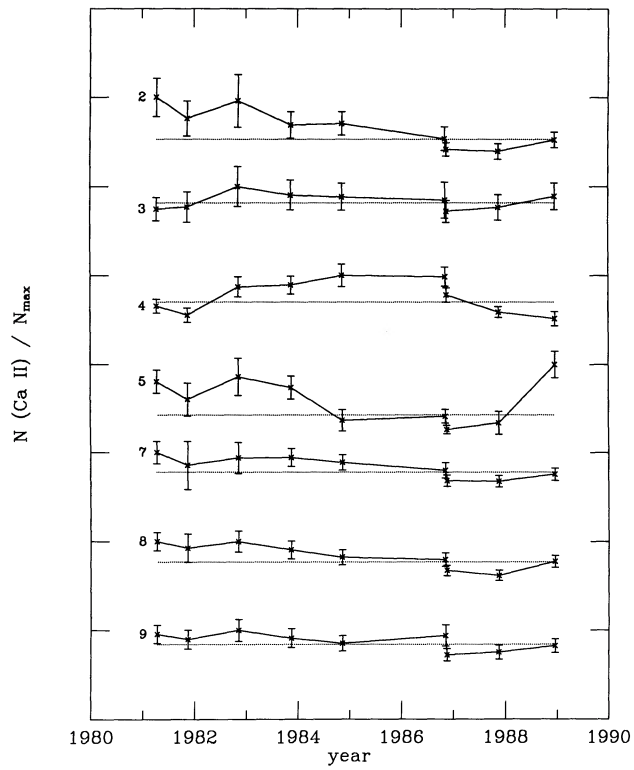

FIG. 7.—The variation with time of the normalized column densities N(Ca II) of the kinematically distinct interstellar clouds seen at the K line. For each cloud, the ratio N/N_{max} is plotted, where N_{max} is the maximum value measured in the nine spectra considered here. The vertical gap between each pair of adjacent tick marks on the vertical axis corresponds to a range from 0.0 to 1.0, and the maximum value attained in each graph is defined to be a ratio of unity. The horizontal dotted lines show the respective average values of the ratios, as weighted by the uncertainties.

3.3. *Results*

Figure 5 shows the variation with time of the total column density, N_{tot}(Ca II), summed over all 10 clouds, as listed near the bottom of Table 2 (in units of 10^{11} cm^{-2}). N_{tot}(Ca II) varied from 1.25×10^{13} to 0.79×10^{13} cm^{-2} in 5 years, between exposures 3 and 8, or by $\sim 45\%$ of its average value determined from all of our spectra. These variations exceed the associated observational uncertainties. Figure 6 shows in more detail the variation with time of the summed column densities of six separate groups of line components, as calculated from Table 2. It will be convenient at times to consider six principal blends of individual components. Blends A, C, and F are defined as the sums of components (1, 2, 3), (5, 6), and (9, 10), respectively, while "blends" B, D, and E redundantly identify components 4, 7, and 8, respectively. It is obvious from Figure 1 that the largest variability arises at radial velocities less than 21 km s^{-1}, i.e., in blends A, B, and, especially, C; even their *relative* intensities vary conspicuously. In particular, despite its very low LSR velocity of about -2 km s^{-1}, blend C displays a nearly negligible relative strength in exposure 7 but becomes the blend of greatest central depth in exposure 9. Furthermore, blends B and C are well resolved in exposures 2 and 3, despite their lower instrumental resolution, and, to a lesser extent, in exposures 4, 6, and 9, while they are effectively indistinguishable in exposures 5 and 8. The discovery of particularly obvious changes of this kind was the principal result previously reported in Paper I. Finally, Figure 7 shows in detail

© American Astronomical Society • Provided by the NASA Astrophysics Data System

1991ApJ...378..586H

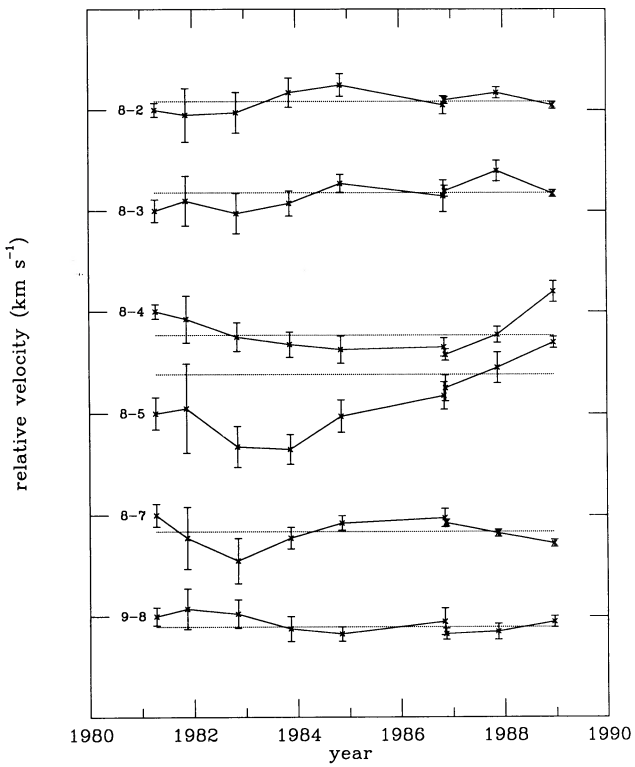

FIG. 8.—The temporal variations, at the Ca II K line, of the radial velocity differences between six interstellar clouds, respectively, and cloud 8. For each of the six pairs of clouds, the difference between the velocity splitting at any time and that measured in spectrum 1 is plotted. The gap between adjacent ticks marks on the vertical axis corresponds to 4 km s^{-1}, and each of the six points for spectrum 1 shows, by definition, a vanishing difference. Each tick mark thus indicates a difference of 0 km s^{-1}. The horizontal dotted lines show the respective average values of the velocity differences, as weighted by the uncertainties.

the variation of the normalized column densities of the individual line components, except that the three weak, strongly blended components (1, 6, and 10), whose column densities are relatively poorly determined, are omitted. The exceptional volatility of blend C is seen to originate almost entirely in component 5; component 6 is much weaker.

From the behavior of component 5, we can speculate on the approximate size of that cloud. Component 5 appeared between 1977 and 1981 and became much weaker during 1984. During 1988 it suddenly strengthened again, although at a radial velocity differing by ~ 4 km s^{-1}. It is therefore possible that the 1988 component revealed a separate cloud. In this interpretation, the size of the previous cloud then was ~ 30 AU, as derived from its lifetime of ~ 5 years and a transverse velocity of 30 km s^{-1}, crudely estimated from a characteristic spread in the observed radial velocities (see, e.g., Wallerstein & Balick 1990).

Figure 8 shows the variation of the radial velocity *differences* between pairs of line components, calculated from Table 2. These differences are independent of any errors which might be present in the zero points of the velocity scales for the various spectra. Components 1, 6, and 10 were omitted again, and component 8 was chosen as the velocity reference for measuring these separations, because its absolute velocity varies minimally and because it is the narrowest well-isolated component. Clouds 4 and 5 show definite variations in relative velocity which exceed the observational uncertainties; the relatively low S/N ratios and the lower instrumental resolution of exposures 1–5 vitiate any attempt to distinguish such variations of the other clouds.

3.4. *Comments*

A transition was made in 1986 from observations obtained near the horizon at McDonald to those acquired more efficiently at ESO, at small zenith distances. The last of these spectra in the north (No. 6) was recorded only 13 days before the first one in the south (No. 7). This interval is far shorter than the gap between any other pair of our K-line exposures. A detailed comparison of these two spectra recorded nearly contemporaneously with completely different instruments may provide useful information about (1) the variability of the K line on a relatively short time scale, (2) the observational errors, if the two profiles essentially agree, or (3) an uncertain mixture of both effects.

The radial velocities may be considered first. The discussion above has addressed the relatively accurately determined differences in velocity between K-line components measured in any one exposure. Figure 8 shows that, for any pair of line components, the respective velocity splittings measured in exposures 6 and 7 indeed agree within their combined uncertainties. In addition, the accuracy of the velocity zero points, or absolute velocity scales, of the two different spectrographs can be estimated by comparing spectra 6 and 7, specifically. Table 2 shows that the absolute velocities deduced for each of the ten clouds toward HD 72127A is, without exception, slightly more positive in exposure 6 than in exposure 7. The average difference of $+0.50 \pm 0.28$ km s^{-1} calculated for the seven line components other than 1, 6, and 10 therefore suggests that a systematic difference of ~ 0.5 km s^{-1} exists between the absolute velocities derived from the two spectrographs. The previous discussion of the relative velocities of line components shown in Figure 8 remains unchanged, but this zero-point offset must be taken into account in comparing absolute velocities which are not measured with the same spectrograph.

The K-line profiles from exposures 6 and 7 are shown together in Figure 9, where a small difference between the relative fluxes is seen most easily near the centers of the absorption lines. The systematically slightly shallower absorption lines deduced from exposure 7 could be caused by a small amount of scattered light in the ESO spectrograph. No independent evidence for such an effect is known to us. Furthermore, the shape of the K line unequivocally varies among exposures 1–6 separately, and among exposures 7–9 separately, for example, so that the temporal variability of the interstellar absorption is indisputable. We will therefore continue to assume that the intensity differences in Figure 9 arise entirely from the intrinsic temporal variation of the absorption, but some small corrections to the equivalent widths and the values of N(Ca II) in spectra 7–9 may be required in the future.

3.5. *Summary*

Unambiguous temporal variability is seen in the total equivalent width of the interstellar K line and in the total Ca II column density derived from it. In more detail, line components 4 and 5, and the associated blends B and C, show variable column densities and radial velocities. Although other clouds among the 10 which were observed are also likely to show real changes, the observational uncertainties enumerated above and the limited number of our spectra do not yet allow us definitely to establish these possible additional effects.

© American Astronomical Society • Provided by the NASA Astrophysics Data System

1991ApJ...378..586H

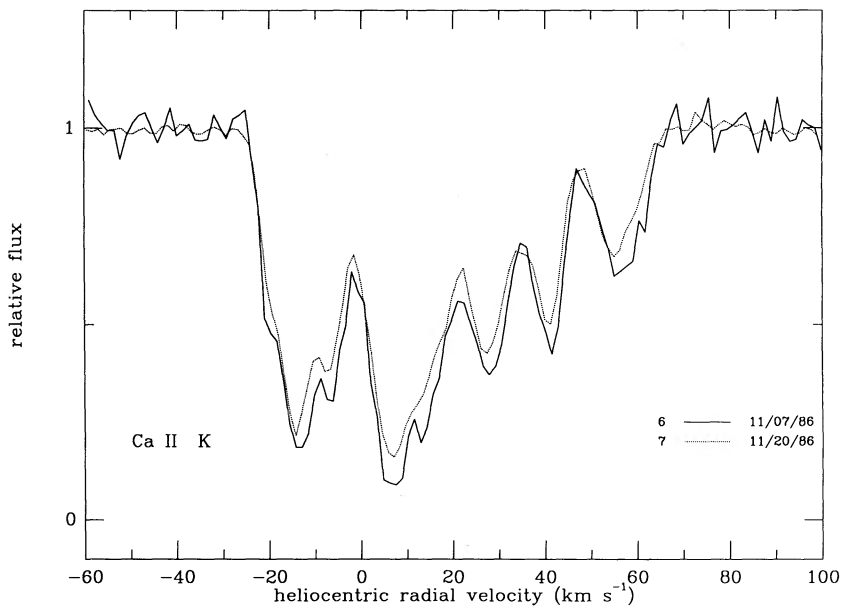

FIG. 9.—A comparison of the K-line profiles in exposures 6 and 7. Exposure 7 show absorption lines which are slightly shallower, as is most easily seen near the line centers.

4. D-LINE PROFILES

4.1. *Overview*

The interstellar D lines in the spectrum of HD 72127A are shown in Figures 3 and 4. The temporal undersampling in these observations is even greater than in those at the K line; the Na I lines have been measured on only four nights from 1981 through 1988. The telluric lines originally present in spectra 12–14 have been removed by dividing each of those spectra by a similar spectrum of α Eri, a telluric standard star. Each auxilairy spectrum was obtained just before or after that of HD 72127A. Although they have not been similarly removed, the few, very weak telluric lines present near the D_1 line in spectrum 11a are only marginally discernible, at S/N $\approx$ 30. The two strongest examples are the features near 43 and 62 km s^{-1}. In contrast, spectrum 11b is affected by three stronger atmospheric features near the D_2 line, exemplified by the especially obvious absorption near 0 km s^{-1}. Data derived from the two interstellar components with which the telluric absorption is blended, which are numbered 3.5 and 6, are enclosed in brackets in Table 3 and will not be used further here.

The most striking feature of the D lines is their extreme weakness relative to the K line (Paper I). Because the strengths of the D lines are in fact roughly "normal" in proportion to the distance and the reddening of HD 72127 (e.g., Hobbs 1974), it is possible that the Na I absorption arises predominantly in ordinary, foreground clouds unrelated to the Vela SNR. We recall, however, that the depletion of sodium from the interstellar gas usually is *much* smaller than that of calcium, so that any enhancement of the D lines in disturbed gas should be correspondingly much less pronounced. Furthermore, at least weak Na I line components are seen over effectively the entire, extremely broad velocity range of the Ca II absorption. This result suggests that a significant fraction of the Na I absorption arises within the gas that also produces the Ca II absorption, especially at the higher velocities. The strongest D-line component occurs at 13 km s^{-1}, or an LSR velocity of -4 km s^{-1}, near which the most highly variable K-line component (No. 5) is found. Despite the low radial velocity of this strongest D-line component, most of the corresponding Na I atoms may therefore reside within the SNR as well. The more detailed results which follow appear to confirm the inferences that most of the Na I and the Ca II absorption occur within the same clouds and that most grains in these clouds have been destroyed.

For each of the Na I spectra, the empirical S/N ratio and the total observed equivalent widths (in mÅ) of the interstellar D_2 and D_1 lines are given near the bottom of Table 3. Just as in the case of the K line, the shapes of the D-line profiles obviously do vary (Fig. 3). However, when the observational uncertainties given for W_λ in Table 3 are taken into account, no unambiguous variability in the total equivalent width of either D line was detectable, if the approximate 2 σ difference in $W_\lambda(D_2)$ between exposures 13 and 14 is ignored.

4.2. *Results*

To permit a more detailed analysis of these data, theoretical multicomponent line profiles have also been fitted to the observations at both Na I lines, just as for the Ca II lines. The results are given in Table 3 and are illustrated in Figures 3, 10, and 11. Because they can be determined from our spectra less accurately than the other values, cloud parameters in Table 3 which are enclosed in parentheses were fixed during the iterative fitting process at the values shown, as was described previously for the Ca II profiles.

Perhaps the most important overall result of this fitting process is contained in the numbering system consequently adopted for the Na I clouds. A minimum of eight distinct interstellar clouds is required to account for all of the unambiguously observed Na I absorption. Table 4 shows that almost every D-line component has a corresponding K-line component which appears at a very similar average velocity. The differences between the respective pairs of average velocities does not exceed 1.5 km s^{-1} in magnitude for most of the clouds, an amount which is comparable to the possible variations of the velocities of the various Ca II components alone.

© American Astronomical Society • Provided by the NASA Astrophysics Data System

1991ApJ...378..586H

TABLE 3

Na I Component Structures

Parameter	Exposure 10 1977 Nov 20 D1	11 1981 Nov 17 D1	11 1981 Nov 17 D2	12 1986 Nov 27 D1	12 1986 Nov 27 D2	13 1987 Nov 28 D1	13 1987 Nov 28 D2	14 1988 Dec 20 D1	14 1988 Dec 20 D2
N2	(0.8)	(0.6)	0.6 ± 0.1	0.8 ± 0.1	0.7 ± 0.1	0.8 ± 0.1	0.9 ± 0.1	0.8 ± 0.1	0.9 ± 0.1
b2	(3.0)	(3.0)	(3.0)	(3.0)	(3.0)	(3.0)	(3.0)	2.5 ± 0.5	2.8 ± 0.3
v2	(−14.6)	(−15.1)	−15.1 ± 0.8	−13.6 ± 0.5	−14.6 ± 0.3	−14.4 ± 0.4	−14.4 ± 0.3	−15.0 ± 0.3	−14.8 ± 0.2
N3	(0.4)	(0.5)	0.5 ± 0.2	0.4 ± 0.1	0.3 ± 0.1	0.4 ± 0.1	0.5 ± 0.1	0.5 ± 0.3	0.4 ± 0.1
b3	(3.0)	(3.0)	(3.0)	(3.0)	(3.0)	(3.0)	(3.0)	3.4 ± 2.0	2.3 ± 0.9
v3	(−7.1)	(−7.6)	(−7.6)	−6.1 ± 1.2	−7.3 ± 0.8	−5.9 ± 1.2	−7.8 ± 0.6	−7.0 ± 1.1	−7.6 ± 0.5
N3.5	2.0 ± 0.6	0.8 ± 0.8	[2.0 ± 0.5]	1.2 ± 0.2	1.4 ± 0.1	1.1 ± 0.1	1.0 ± 0.1	1.1 ± 0.4	1.3 ± 0.4
b3.5	(3.0)	(3.8)	[3.2 ± 1.2]	(3.8)	(3.8)	(3.8)	(3.8)	3.3 ± 1.3	4.4 ± 1.3
v3.5	1.3 ± 1.1	1.6 ± 3.7	[−0.4 ± 0.7]	1.7 ± 0.8	0.4 ± 0.4	0.2 ± 1.0	−0.2 ± 0.6	0.4 ± 0.5	0.3 ± 0.6
N4	4.5 ± 0.9	2.5 ± 1.1	3.5 ± 0.6	4.5 ± 0.2	4.4 ± 0.2	3.4 ± 0.2	3.1 ± 0.1	3.2 ± 0.1	3.2 ± 0.2
b4	2.5 ± 0.7	2.0 ± 1.4	2.3 ± 0.7	1.6 ± 0.2	2.3 ± 0.2	(4.0)	(4.0)	(4.0)	(4.0)
v4	6.7 ± 0.4	6.3 ± 0.5	6.4 ± 0.3	7.3 ± 0.1	7.1 ± 0.1	7.4 ± 0.4	7.4 ± 0.3	7.8 ± 0.4	7.9 ± 0.4
N5	9.8 ± 2.1	10.5 ± 0.9	7.2 ± 0.5	8.7 ± 0.4	5.0 ± 0.3	6.6 ± 0.2	3.3 ± 0.2	12.0 ± 0.4	9.0 ± 0.4
b5	1.8 ± 0.3	2.5 ± 0.4	2.4 ± 0.3	(1.5)	1.4 ± 0.2	(1.5)	(1.5)	(1.5)	(1.5)
v5	13.1 ± 0.2	13.1 ± 0.2	13.1 ± 0.2	12.6 ± 0.1	12.5 ± 0.1	12.7 ± 0.1	12.7 ± 0.1	12.6 ± 0.1	12.6 ± 0.1
N6	3.6 ± 1.9	1.4 ± 0.5	[2.9 ± 0.3]	2.3 ± 0.3	2.8 ± 0.2	3.4 ± 0.2	2.8 ± 0.2	2.2 ± 0.3	2.0 ± 0.2
b6	(3.5)	(5.0)	(5.0)	(5.0)	(5.0)	(5.0)	(5.0)	3.9 ± 0.6	3.7 ± 0.3
v6	16.1 ± 1.4	20.2 ± 2.1	[20.2 ± 0.5]	16.3 ± 0.6	16.3 ± 0.3	18.0 ± 0.3	17.0 ± 0.3	17.0 ± 0.5	17.6 ± 0.3
N7/8	(1.2)	(1.2)	1.2 ± 0.2	1.0 ± 0.1	1.1 ± 0.1	1.6 ± 0.1	1.6 ± 0.1	1.4 ± 0.1	1.2 ± 0.1
b7/8	(7.0)	(7.0)	(7.0)	(7.0)	(7.0)	(7.0)	(7.0)	(7.0)	(7.0)
v7/8	(34.5)	(35.3)	35.4 ± 1.0	34.6 ± 1.0	34.6 ± 0.5	33.0 ± 0.6	32.7 ± 0.4	35.5 ± 0.4	33.3 ± 0.3
N9	(0.4)	(0.4)	0.4 ± 0.1	(0.4)	0.4 ± 0.1	0.4 ± 0.1	0.5 ± 0.1	0.7 ± 0.1	0.4 ± 0.1
b9	(5.0)	(5.0)	(5.0)	(5.0)	(5.0)	(5.0)	(5.0)	(5.0)	(5.0)
v9	(54.0)	(53.0)	53.0 ± 1.8	(53.2)	52.9 ± 0.8	54.8 ± 1.1	54.5 ± 0.7	54.9 ± 0.4	53.7 ± 0.6
S/N	15	30	30	70	70	70	80	130	180
W_λ	>131	>111	<271	148 ± 6	229 ± 6	154 ± 6	221 ± 5	154 ± 3	237 ± 2
N_{tot}	22.7	17.9	18.3	19.3	16.1	17.7	13.7	21.9	18.4
rms	0.069	0.034	0.026	0.012	0.013	0.011	0.016	0.006	0.009

TABLE 4

Average Properties of Line Components

Component	Blend	V_{LSR}(Ca II) (km s^{-1})	$V_\odot$(Ca II) (km s^{-1})	$V_\odot$(Na I) (km s^{-1})	N(Ca II) (10^{11} cm^{-2})	N(Na I) (10^{11} cm^{-2})	N(Ca II)/N(Na I)
1	...	−36.0	−19.1	...	4.5	<0.08	>56.
2	...	−31.2	−14.3	−14.6	11.9	0.8	14.9
3	...	−24.6	−7.7	−7.4	12.9	0.4	32.3
3.5	...	...	...	0.4	...	1.2	...
4	...	−10.9	6.0	7.2	21.6	3.4	6.4
5	...	−4.2	12.7	12.7	8.8	6.2	1.4
6	...	0.6	17.5	17.2	4.4	2.6	1.7
7	...	10.8	27.7	...	13.3	...	...
7/8	...	...	...	33.9	...	1.3	...
8	...	23.4	40.3	...	7.9	...	...
9	...	38.4	55.3	54.1	5.6	0.4	14.0
10	...	44.3	61.2	...	0.3	<0.08	>3.8
1 + 2 + 3	A	...	...	...	29.5	1.8	16.4
4	B	...	...	...	21.6	4.0	5.4
5 + 6	C	...	...	...	13.2	8.8	1.5
7	D	...	...	...	13.3	0.65	20.5
8	E	...	...	...	7.9	0.65	12.2
9 + 10	F	...	...	...	5.9	0.4	14.8
All	Total	...	...	...	91.4	16.3	5.6

© American Astronomical Society • Provided by the NASA Astrophysics Data System

1991ApJ...378..586H

Most of the identifying numbers previously assigned to the Ca II components will therefore be carried over to the corresponding Na I features as well. Exceptions are the Na I cloud numbered 3.5, which has no clearly resolved Ca II counterpart, and the weak, broad, apparently unresolved Na I component numbered 7/8. This component occurs at a velocity near the average of the two narrower, well-resolved Ca II components numbered 7 and 8. An inspection of the data yields little physical basis for associating these two Ca II components with the Na I component; it is more likely that these are actually three physically distinct clouds with widely different Ca II/Na I ratios. Nevertheless, to avoid an uncertain proliferation of the separately identified clouds here, D-line component 7/8 will generally be compared below with the K-line components 7 and 8 together. Finally, no detectable Na I absorption is seen at the velocities of the very weak, blended Ca II components numbered 1 and 10. The upper limits on N(Na I) listed in Table 4 for these two components were derived from exposure 14.

Figure 10 shows the variation with time of the total Na I column density, N_{tot}(Na I), summed over all eight clouds, as listed near the bottom of Table 3 (in units of 10^{11} cm^{-2}). For each cloud in each of spectra 11–14, the average of the column densities derived from the two D lines has been used, except as precluded by telluric interference in spectrum 11. In comparison with the K-line column densities, the enhanced accuracy provided by using this average value partially compensates for the lower accuracy with which the column densities of the weakest D-line components can be determined, even at the relatively high S/N ratios achieved in the ESO spectra. The unweighted average of these 25 individual ratios is $\langle N(D_1)/N(D_2)\rangle = 1.13 \pm 0.33$; this average becomes

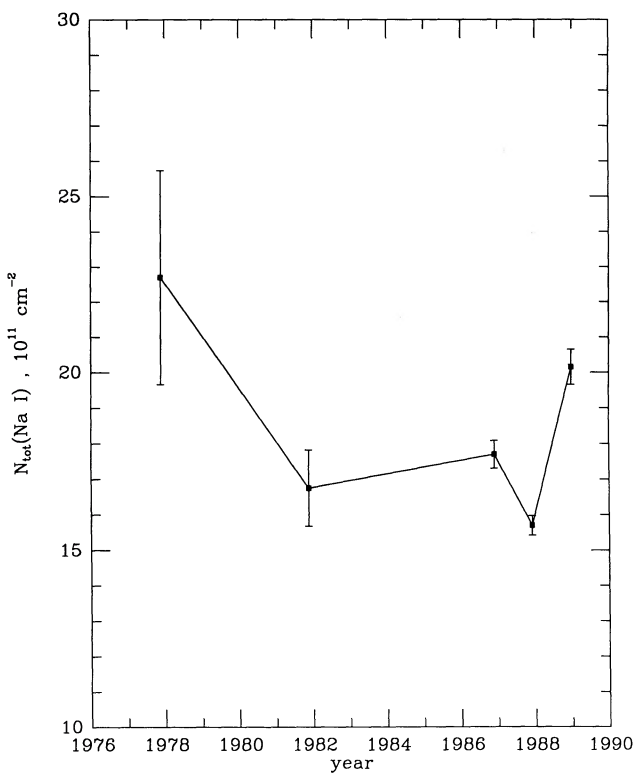

FIG. 10.—The variation with time of N_{tot}(Na I), the total column density of interstellar Na I along the light path to HD 72127A.

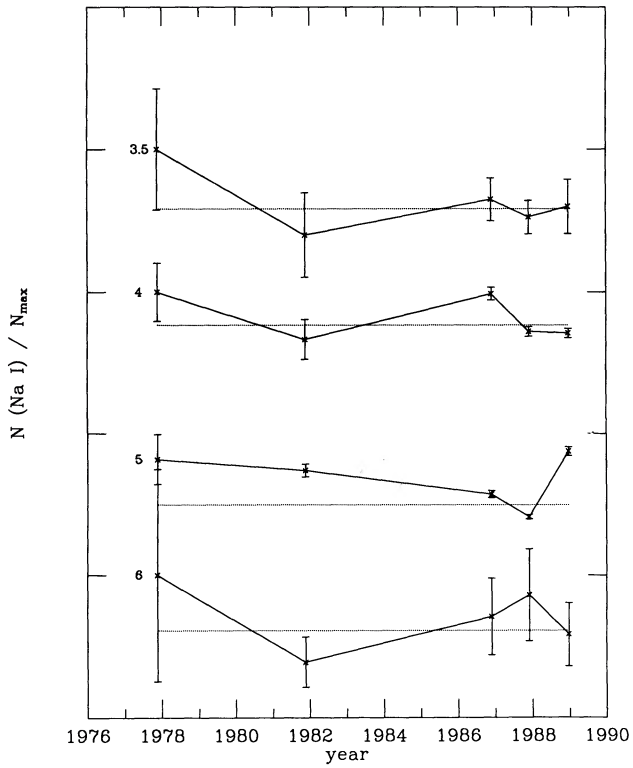

FIG. 11.—The variation with time of the normalized column densities N(Na I) of four of the kinematically distinct interstellar clouds seen at the D lines. For each cloud, the ratio N/N_{max} is plotted, where N_{max} is the maximum value measured in the spectra considered here. The vertical gap between each pair of adjacent tick marks on the vertical axis corresponds to a range from 0.0 to 1.0, and the maximum value attained in each graph is defined to be a ratio of unity. The horizontal dotted lines show the respective average values of the ratios, as weighted by the uncertainties. For exposures 12–14, the averages of Na I column densities obtained from the D_1 and the D_2 are shown.

1.03 ± 0.23 for 21 individual ratios, when the strongest D-line component, No. 5, is excluded. The derived total column density N_{tot}(Na I) shows a definite variation from 2.3×10^{12} to 1.6×10^{12} cm^{-2} in 10 years, between exposures 10 and 13, or by $\sim$38% of its average value determined from all of our spectra. This variation exceeds the observational errors. The extreme temporal undersampling of our data also must be emphasized once again.

Figure 11 further shows in detail the variation of the normalized column densities of the four strongest individual D-line components, which probably have been deduced with the highest accuracy. Clouds 4 and 5 together typically contain approximately two-thirds of the total Na I column density. The column densities N(Na I) in these two clouds show definite variations between spectra 12 and 13.

When the radial velocity differences among the various Na I clouds are considered, no definite temporal variations which exceed the associated observational uncertainties are found. The absence of detectable variations for clouds 4 and 5, which contrasts with the definite velocity variations seen for these two clouds at the K line, may indicate some contamination of this Na I absorption by foreground material. Fairly strong D-line absorption, which corresponds to N(Na I) = 1.3×10^{12} cm^{-2} or $\sim$65% of the total seen toward HD 72127A, is in fact found at $v_{LSR} \approx 1$ km s^{-1} toward HD 72232 (Wallerstein, Silk, & Jenkins 1980), an apparent foreground star which is located $\sim 1^\circ.5$ from HD 72127 on the sky, at $d \approx 240$ pc. Most of the

© American Astronomical Society • Provided by the NASA Astrophysics Data System

1991ApJ...378..586H

other stars closer than 300 pc which were observed in that survey show lower column densities, $N(\text{Na I}) \lesssim 4 \times 10^{11}$ cm^{-2}.

4.3. *Summary*

Unambiguous temporal variability is seen in the shape of the interstellar D lines and in the total Na I column density derived from them, although their total equivalent widths are accidentally invariant to within the observational errors. In more detail, line components 4 and 5 show variable column densities, in agreement with the previous results at the K line.

5. DISCUSSION

In Paper I, we emphasized (1) the temporal variation of the total equivalent width of the interstellar K line in the spectrum of HD 72127A, (2) the variable degree of resolution between blends B and C at the K line, and (3) the large column-density ratios $N(\text{Ca II})/N(\text{Na I})$ measured for five of the six principal line blends at the K line. Obtained with digital detectors, our new spectra are more numerous and can be more easily intercompared quantitatively. They confirm and extend all three of the earlier results. A brief rediscussion of the third point is appropriate.

The average column densities of Ca II and Na I contained within each of the individual K-line components and in each of their six principal blends are listed in Table 4. For simplicity in these comparisons, the relatively small column density of Na I seen in cloud 3.5 has been reallocated in equal halves to clouds 3 and 4. Similarly, but with less justification (§ 4.2), the column density of Na I seen in cloud 7/8 has been divided equally between clouds 7 and 8, separately. Five of these six principal line blends of K-line components show $N(\text{Ca II})/N(\text{Na I}) > 5.4$. Within the Galaxy, such a result is approximately duplicated outside the region of the Vela SNR only along the much longer light path to HD 14633 (Hobbs 1983), to our knowledge. Only a small fraction of the interstellar line components seen toward other stars appear to show well determined ratios $N(\text{Ca II})/N(\text{Na I}) > 5$, which can be considered the extreme domain of the Routly-Spitzer effect (Siluk & Silk 1974; Cowie & York 1978). A possibly similar complex of interstellar lines was seen by Jenkins, Silk, & Wallerstein (1984) toward HD 72089, another star associated with the Vela remnant. On photographic echelle spectra with dispersions of 2.2 and 3.3 Å mm^{-1} at the Ca II and Na I lines, respectively, six components were seen with $N(\text{Ca II})/N(\text{Na I})$ ratios ranging from less than 6.3 to more than 15.8.

These conclusions are based on the time-averaged ratios of column densities, because we did not obtain observations of both Ca II and Na I on any one night. Significant variations in the interstellar absorption may possibly occur over even the shortest such intervals so far sampled, which amount to the several days between spectra 2 and 11 and between spectra 9 and 14. Furthermore, in view of the very complex arrays of blended line components seen in our data, some of the components which appear unresolved at our instrumental resolutions may actually consist of several additional, blended, narrower, temporally variable components whose *relative* intensities may differ markedly between the Ca II and the Na I lines. Specific evidence for such unresolved component structure exists in the case of cloud 4, for example. Tables 2 and 3 show that $b(\text{Ca II}) > b(\text{Na I})$ for this cloud, a result which cannot be explained by any combination of thermal and "turbulent" line broadening within a single cloud. Observations at still higher resolution therefore may be needed in order to make proper comparisons between the Ca II and Na I profiles. With these cautionary statements in mind, Figure 12 nevertheless shows the detailed time variation of the ratios $N(\text{Ca II})/N(\text{Na I})$ for four of the principal line blends. In all cases, the Na I data have been combined with the most nearly contemporaneous Ca II data available. Line components 7 and 8 ("blends" D and E, respectively) have been omitted from the figure, owing to the uncertain correspondence between these two K-line components and D-line component 7/8 (§ 4.2). If all error estimates shown in Figure 12 were increased by the relatively small factor of ~ 1.7, no variability of the respective $N(\text{Ca II})/N(\text{Na I})$ ratios in excess of the observational errors would remain. In view of this fact and of the temporal gaps between the paired observations of the Ca II and the Na I lines, no definite evidence of such variability can safely be deduced from our relatively few, existing spectra. Figure 13 compares directly the profiles of the K line and the D_2 line, for each of the four most nearly simultaneous pairs of such observations; the differences in resolution (Table 1) and in S/N ratio (Tables 2 and 3) among the various spectra must again be taken into account.

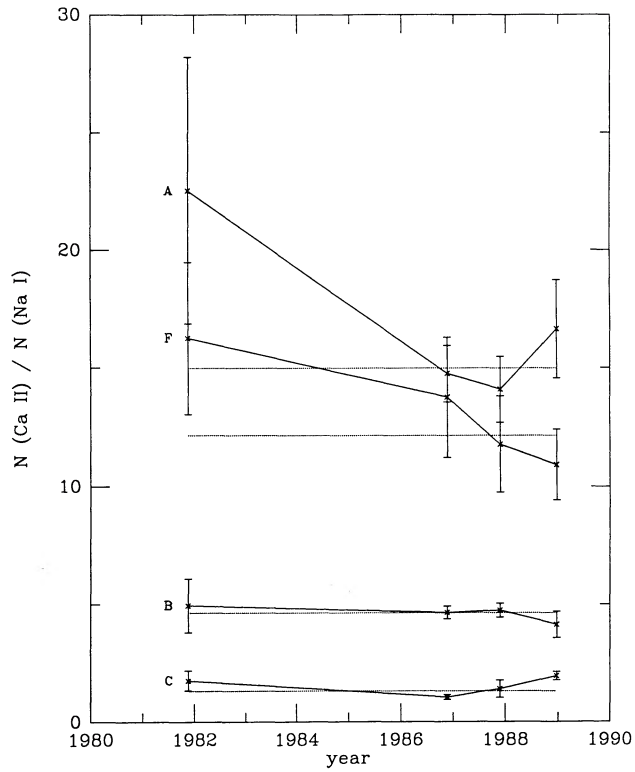

FIG. 12.—The variation with time of the column-density ratio $N(\text{Ca II})/N(\text{Na I})$, for four of the principal K-line blends. In all cases, the Na I data have been combined with the most nearly contemporaneous Ca II data available from our spectra.

The large Ca II/Na I ratios seen toward HD 72127A can be interpreted most easily as evidence for "anomalously" large Ca/Na abundance ratios in the absorbing gas (Jenkins, Silk, & Wallerstein 1976; Paper I; Hobbs 1983). This hypothesis is strengthened by the fact that, except for cloud 7, the largest Ca II/Na I ratios are seen at the highest observed LSR velocities, $|v_{\text{LSR}}| \geq 23$ km s^{-1} (Table 4). The dominant destruction mechanism for refractory grains such as those containing calcium probably is interstellar shock waves, mainly through

© American Astronomical Society • Provided by the NASA Astrophysics Data System

1991ApJ...378..586H

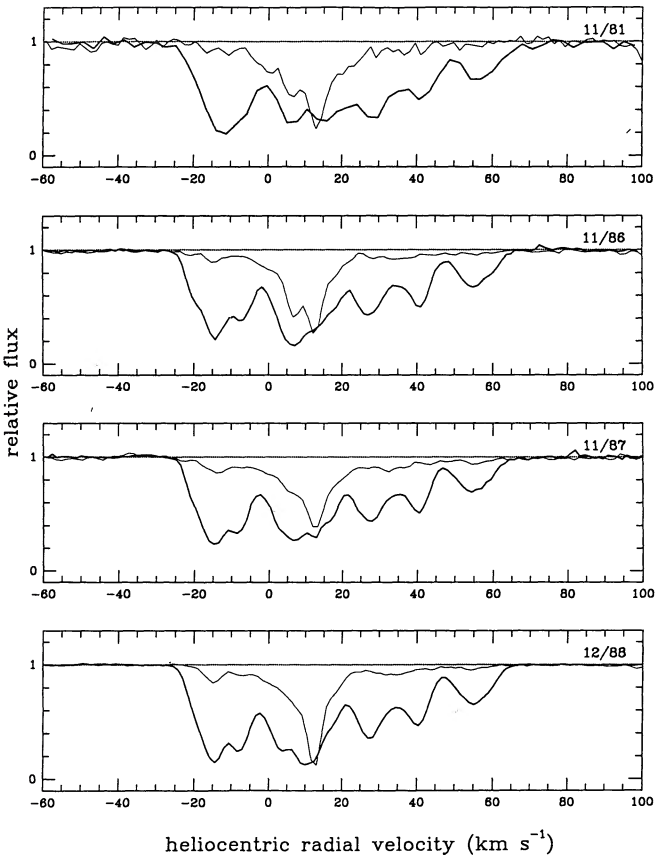

FIG. 13.—The profiles of the K line and the D_2 line in the spectrum of HD 72127A, for each of the four most nearly simultaneous pairs of exposures available (Table 1). The observations were obtained in 1981 November, 1986 November, 1987 November, and 1988 December, respectively.

the mutual collisions of charged grains as they spiral along magnetic field lines (Draine & Salpeter 1979; Seab & Shull 1983; McKee et al. 1987). Although the radial velocities seen toward HD 72127, $|v_{LSR}| \leq 39$ km s^{-1} except for cloud 10, are somewhat lower than those often required to enhance markedly the Ca II/Na I ratio (Siluk & Silk 1974), these radial components are only lower limits to the true velocities. The theoretical studies cited above have emphasized that shock waves with initial velocities in excess of only 40 km s^{-1}, or perhaps 50 km s^{-1}, can effectively destroy the larger interstellar grains. Low-velocity absorption by highly ionized species is indeed detected toward the Vela SNR; in particular, C IV absorption toward HD 72127A is found at the velocity of cloud 8. The C IV ions could be created either by collisional ionization in the conductive boundary layers behind a shock front or through photoionization by UV radiation from the shocked gas. The latter radiation also can directly enhance the destruction of grains.

In general terms, the most important reason for further extending such observations of HD 72127 is to refine the direct, presently unique knowledge so provided about the time scales on which the observed variations can occur. For the reasons indicated above, future efforts should incorporate much more frequent observations of both the Ca II and the Na I absorption, always obtained effectively simultaneously and at still higher spectral resolution. Suitable observations of some foreground stars would further permit at least a partial removal of any foreground absorption which contributes to the observed profiles. Such a more comprehensive data set will be required in order to surmount reliably most of the remaining interpretive limitations which are imposed by the present spectra.

It is a pleasure to thank the staffs of the McDonald and the ESO observatories for their help and hospitality, and to acknowledge financial support for this work through grants NGR 14-001-147 and NAGW-1475 from the National Aeronautics and Space Administration to the University of Chicago.

REFERENCES

Blades, J. C. 1976, MNRAS, 177, 79
Cowie, L. L., & York, D. G. 1978, ApJ, 223, 876
Draine, B. T., & Salpeter, E. E. 1979, ApJ, 231, 438
Ferlet, R., & Dennefeld, M. 1984, A&A, 138, 303
Hobbs, L. M. 1974, ApJ, 191, 381
———. 1978, ApJS, 38, 129
———. 1979, PASP, 91, 690
———. 1983, ApJ, 265, 817
———. 1984, ApJS, 56, 315
Hobbs, L. M., Wallerstein, G., & Hu, E. M. 1982, ApJ, 252, L17 (Paper I)
Jenkins, E. B., Silk, J., & Wallerstein, G. 1976, ApJS, 32, 681
———. 1984, ApJ, 278, 649
McKee, C. F., Hollenbach, D. J., Seab, C. G., & Tielens, A. G. G. M. 1987, ApJ, 318, 674
Seab, C. G., & Shull, J. M. 1983, ApJ, 275, 652
Siluk, R. S., & Silk, J. 1974, ApJ, 192, 51
Thackeray, A. D. 1974, Observatory, 94, 55
Vidal-Madjar, A., Laurent, C., Bonnet, R. M., & York, D. G. 1977, ApJ, 211, 91
Vidal-Madjar, A., Hobbs, L. M., Ferlet, R., Gry, C., & Albert, C. E. 1986, A&A, 167, 325
Wallerstein, G., & Balick, B. 1990, MNRAS, 245, 701
Wallerstein, G., Silk, J., & Jenkins, E. B. 1980, ApJ, 240, 834
Welty, D. E., Hobbs, L. M., & York, D. G. 1991, ApJS, 75, 425

© American Astronomical Society • Provided by the NASA Astrophysics Data System